Infrared Imaging Spectroscopic System for the Detection of Skin Cancer: Preliminary results

Laura Rey[1], Francisco J. Burgos-Fernández[1], Xana Delpueyo[1], Miguel Ares[1], Santiago Royo[1], Josep Malvehy[2], Susana Puig[2], Meritxell Vilaseca[1]*

[1] Centre for Sensors, Instruments and Systems Development, Technical University of Catalonia; Terrassa, Spain

[2] Dermatology Department of the Hospital Clinic of Barcelona, IDIBAPS; Barcelona, Spain

Abstract

Skin cancer is a disease of the twenty-first century mainly caused by the excessive exposure to the sun without the appropriate solar protection. Melanoma, which is one of the most aggressive kinds of skin cancer, requires a rapid and effective diagnosis. Clinical examination and biopsies have shown to be slow and costly in many ways, so the possibility of getting a non-invasive optical detection of skin melanomas became a hot topic in biophotonics. In this context, multispectral imaging systems have approached the problem, but none of them worked inside the infrared range yet. Hence, this work has been proposed as an interesting, long-term project to further investigate about the possibilities of infrared imaging spectroscopy for the early detection of skin cancer, especially melanomas.

Introduction

Skin cancer is the uncontrolled growth of abnormal skin cells. It occurs when unrepaired DNA damage to skin cells triggers mutations or genetic defects that lead the skin cells to multiply rapidly and form malignant tumors [1]. Surprisingly, in the past three decades, more people have had skin cancer than all other cancers combined [2].

The development of skin cancer or pre-cancer can be identified clinically when a mole, a birthmark, a beauty mark or a brown spot changes its color, increases its size or thickness, and gets an unusual texture or its outline gets irregular. In the diagnosis process, the first contact is visual and unless the clinical exam draws very firm conclusions, a skin biopsy is required. It is a long-term process which can take two or three weeks that involves a surgical procedure and a histologic analysis [3]. Due to the large number of affected people, there have been many research efforts against skin cancer, in order to better suggest the diagnosis of malignant lesions beyond classical dermoscopy and avoiding unnecessary biopsies. An approach that might be suitable is multispectral imaging because of the spectral and spatial capabilities it offers. Examples range from the spectral analysis through a microscope to obtain information on tissue allowing different molecules to be differentiated despite being superimposed (Schultz et al. 2001); the detection of subcutaneous veins for the insertion of intravenous catheters with the aid of a near infrared source (Meriaudeau et al. 2009); the oxygen blood flow and saturation measurement and the intracellular calcium dynamics assessment (Basiri et al. 2010; Bouchard et al. 2009); and systems for the diagnosis of retinal diseases and the oxygen saturation maps measurement (Everdell et al. 2010; Gao et al. 2012; Khoobehi et al. 2004) (Figure 2.15). Other medical applications include the diagnosis of diseases through the spectral study of the tongue (Liu et al. 2007)and the diagnosis of cancer. In this context, attempts have been made to achieve automatic detection of white blood cells in the bone marrow (Guo et al. 2007), improve diagnosis of prostate cancer (Akbari et al. 2012), cervical cancer (Thekkek & Richards-Kortum 2008) or gastric cancer (Kiyotoki et al. 2013), among others. Furthermore, spectral imaging systems have also been used in the detection of skin cancer lesions and they are explained next.This technique provides a precise quantification of the spectral, colorimetric and spatial features of skin lesions that are caused by chromophores such as melanin, hemoglobin and water, which might differ among skin lesions of different etiologies.

Multispectral systems (MS) have proved that they are capable of analyzing reliably and non-invasively the presence of chromophores as fingerprints of any pathology. Different research groups have approached the problem of skin cancer detection with multispectral devices [4, 5, 6].

In 2005, Tomatis et al. [4] developed an automated diagnosis of pigmented lesions. The device consisted of a spectrophotometer with a light source, a monochromator and a bundle of optical fibers coupled to the probe head. The spectral range from 483 nm to 950 nm was covered with 15 spectral bands. A region growing algorithm segmented the lesions and extracted descriptors to be used as input for setting and testing a neural network classifier.

Some years later, in 2011, Kuzmina et al. [5] used a MS that incorporated halogen lamps and filters from 450 nm to 950 nm with a spectral bandwidth of 15 nm. They observed that wavelengths closer to the infrared (IR) range penetrate deeper in the skin, resulting in a decreased contrast due to higher light scattering. However, in the case of melanomas at 950 nm the contrast was found to be much higher, indicating considerably deeper structural damage of skin. The fact that melanomas damage the skin deeply could be a hint to explore further on the IR as this radiation penetrates more at some wavelengths in this range.

In 2012, Bekina et al. [6] analyzed lesions under a MS with four different spectral bands, each one to obtain information from specific structures of the skin: 450 nm for superficial layers; 545 nm for blood distribution; 660 nm melanin detection and 940 nm for the evaluation of deeper skin layers. Then, a ratio was calculated between the intensities in green light (560 nm), where the hemoglobin absorption is high, and red light (650 nm), where it is low. It was proven that pathological tissues showed higher values of this index than the surrounding skin as a consequence of having higher blood content.

In this sense, in a previous work we developed a handheld multispectral imaging system based on a CCD camera with eight spectral bands from 414 nm to 995 nm as a part of the European Project DIAGNOPTICS "Diagnosis of skin cancer using optics" (ICT PSP seventh call for proposals 2013) [7]. The goal of this project was the development of multi-photonic diagnostic platform including multispectral and 3D techniques [8], blood flow analysis based on self-mixing [9] and confocal microscopy [10] for in-vivo imaging of skin cancer lesions. The main objectives of the present

study (Spanish Ministry of Economy, Industry and Competitiveness under the grant DPI2014-56850-R) is to further investigate about the possibilities of a multispectral imaging system for the detection of skin cancer, especially melanoma, in the IR range from 970 nm to 1550 nm by means of a InGaAs camera. Since these wavelengths deeply penetrate into the tissue, they may release information about how deeper tissues are damaged due to UV radiation, water content, and other factors which might be different in benign and malignant lesions.

Methods

Experimental Setup

The device developed integrates a 16-bit depth InGaAs camera (Hamamatsu C10633-23) with spectral sensitivity from 900 nm to 1600 nm and 320x256 pixels together with a Kowa LM12HC-SW 1.4/12.5 mm SWIR lens with high transmission from 800 nm to 2000 nm. Additionally, a LED-based light source was built on a cylinder of Polyvinyl chloride (PVC) with peak wavelengths at 970 nm, 1050 nm, 1200 nm, 1350 nm, 1450 nm and 1550 nm. The tip of the cylinder is a cone with an opening of 2 cm x 2 cm and a diffuser. Four light-emitting diodes (LEDs) per spectral band were included in the light source with a separation of 90º among them to ensure a uniform illumination over the skin; a total amount of 24 LEDs were finally placed on the ring. All parts were assembled in a handheld configuration with a trigger to start the acquisition (Fig. 1). A base of PVC was also designed and constructed to hold the MS when it is not being used. It incorporates a calibrated reference at the bottom which consist in the Neutral 5 gray color of a X-Rite ColorChecker® with level of reflectance similar to that of the skin in the IR.

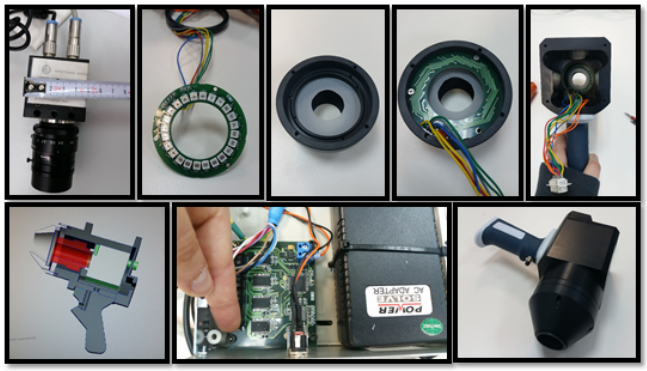

***Figure 1**. Handheld IR MS.*

Acquisition protocol

The acquisition software was based on Borland Builder C++ and it was built with a friendly interface for physicians. The software controls individually and synchronously the emission of the LEDs and the acquisition by means of the IR camera to obtain sequence of images. The software interface first asks for a calibration every day before making any measurements. It involves a sequence of acquisition of images for the reference at the six spectral bands and at ten different exposure times taking into account the LED emission level and also the typical reflectance and absorption properties of the skin. In total, 60 calibration images are acquired.

Then a measurement over the actual skin can be done, and the system will make a sequence of six acquisitions, at six different spectral bands. Each one is acquired with a given exposure time, according to a reference average that has to be reached. Eventually, other 60 dark current images need to be acquired by just making another calibration in dark conditions, to take into account the noise sensed by the camera at the time of calculating the reflectance curve of a pixel area. The software also includes security controls avoiding LEDs to be switched on if the program is not running.

Image processing

The images were then processed through a graphical user interface (GUI) built in Matlab R2015a (Fig. 2). It has different functions to make internal calibration algorithms and also computes reflectance spectra that can be used to compare subtle differences between benign and malignant lesions.

Reflectance reconstruction

In order to calculate the reflectance images, the corresponding calibration images from the references and dark current images are selected by the program. Then, reflectance at each pixel *(i,j)* on the cube is calculated as follows:

$$I_R(i,j) = k \frac{I(i,j) - I_D(i,j)}{I_N(i,j) - I_D(i,j)}. \quad (1)$$

For a given acquisition channel, $I_R(i,j)$ is the spectral reflectance image; $I(i,j)$, $I_N(i,j)$, and $I_D(i,j)$ contain the digital levels of the raw, neutral reference and dark images, respectively; k is the calibrated reflectance of the reference used, provided by the manufacturer.

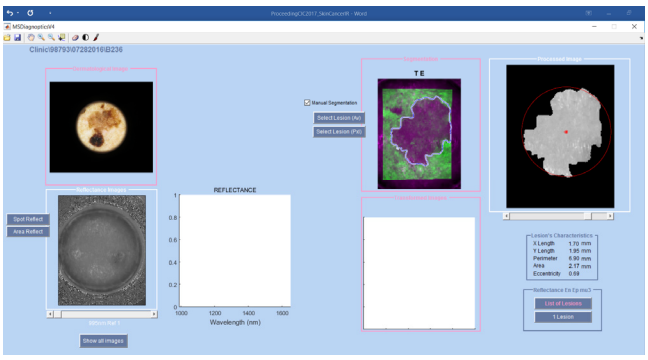

***Figure 2**. Matlab GUI for reflectance reconstruction, segmentation of lesions and calculation of descriptors.*

Image registration and segmentation

Since the purpose was to obtain information about the lesions themselves, and not from their hole reflectance images (which contain spectral information about the healthy skin too), every lesion was segmented away from their six spectral images.

The method used was manual segmentation over the lesion and its corresponding visible reflectance image correlated to it, which was obtained from another MS with illumination in the visible range. The registration of the images from both systems was required since it was proved that some lesions could not be properly seen in some spectral bands of the IR range due to their spectral and texture characteristics; hence, their segmentation was difficult in this region neither automatically nor manually. Fortunately, the lesions were also measured under a visible MS at the same position and in the same orientation over the patients' skin thanks to a metallic ring that attaches to the skin while taking the spectral images and over which the opening of both systems can be placed.

Statistical descriptors

An image of the segmented lesion was obtained for each spectral image. In addition, another image was calculated as the image of the segmented lesion minus the average reflectance of the patient´s skin, to prevent it from influencing the results. Finally, another two pair of images were also calculated as the logarithm of the latter ones, in order to obtain information in terms of absorbance.

The whole set of the aforementioned images was evaluated through the following mathematical descriptors: mean (μ), standard deviation (σ), energy (*En*), entropy (*Ep*), and third central moment (μ_3). The last three statistical descriptors are based on the histogram of the image values and are defined as follows,

$$En = \sum_{i=0}^{N-1} P(i)^2, \tag{2}$$

$$Ep = -\sum_{i=0}^{N-1} P(i)\ \log_2[P(i)], \tag{3}$$

$$\mu_3 = \sum_{i=0}^{N-1} (i-\mu)^3 P(i), \tag{4}$$

Where *P(i)* is the value (frequency) of the intensity element *i* (bin) of the histogram; *N* is the number of levels that the histogram is divided into.

Energy is a numerical descriptor of the image uniformity that ranges between 0 and 1, reaching the maximum value for a constant image [11]. In regard to entropy, it is a well-known statistical measure of randomness, uncertainty or disorder in image values, being 0 the minimum value for a constant image, and $log_2(N)$ the maximum [11]. It can be noticed that these two descriptors are inversely related. The third central moment or skewness, μ_3, refers to the skewness of the histogram about its mean; it has a range of values between -1 and 1, positive for histograms skewed to the right about the mean, negative for the ones skewed to the left, and 0 for symmetric ones [11]. According to all this, these descriptors can be used to account for textural features of skin lesions besides the more classical spectral information obtained from traditional MS.

Mean, standard deviation, energy, entropy and skewness for the four aforementioned images resulted into 30 different descriptors for each spectral band. Since our system provides six spectral bands, the total number of descriptors to be analyzed was 180. In order to determine which descriptors were useful as classifiers we plotted the values for every one of the 180 descriptors of a set of lesions in which 28 nevi and 11 melanomas were included.

Upper and lower thresholds were experimentally defined in the plots as the interval limits that included melanomas or possible nevi depending on the algorithm applied. Consequently, the lesions that fell outside the thresholds for at least one parameter were considered to be nevi or melanomas.

Results and Discussion

Clinical measurements of real skin lesions, including benign and malignant ones (essentially melanomas) were acquired under the supervision of expert physicians at the Hospital Clinic of Barcelona. All patients provided written informed consent before any examination and ethical committee approval was obtained. The study complied with the tenets of the 1975 Declaration of Helsinki (Tokyo revision, 2004).

A large set of lesions was acquired and diagnosed by means of a dermoscope, a commercial confocal laser scanning microscope and biopsy when needed. However, some lesions could not be segmented from the skin with our processing software for two reasons: some of their corresponding images in the visible range were missing, which are needed to perform image registration and segmentation. Also because in some instances, the metallic ring was moved while switching from one system to the other, and hence the images could not be properly correlated.

Only perfectly defined and segmented lesions were included in the study to ensure accurate results, even though it led to a small set of lesions. Other lesions that were collected had a different diagnosis than those aforementioned such as basal cell carcinoma and seborrheic keratosis, and hence, they were not included in this analysis.

The average reflectance of the nevi is known to be higher with respect to the melanoma population in the visible range [12], although the ±σ, standard deviation of the data that was analyzed made it quite entangled.

As it can be seen in Fig. 3, the mean reflectance of both populations in the infrared range is separated from each other one standard deviation, approximately, being that of nevi especially higher from 995 nm to 1350 nm than for melanomas.. This wavelength range corresponds to that in which radiation can penetrate deeper into the tissue (longer wavelengths are highly absorbed by water) and thus, can inform of deeper structures which could be notably different between nevi and melanomas.

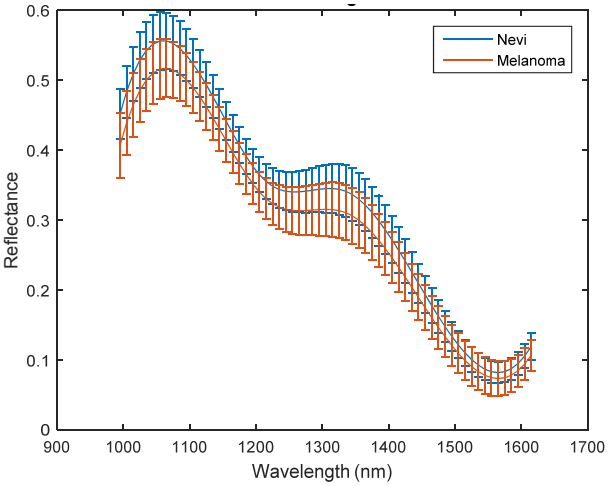

***Figure 3**. Average reflectance infrared spectra of nevi and melanomas.*

Histograms for nevi and melanoma lesions were also compared. Fig. 4 shows two representative histograms of a nevus and a melanoma in terms of reflectance at 1214 nm. The averaged spectral reflectance, the standard deviation and corresponding *Ep*, *En*, and μ_3 are also shown.

Here, we can see that the *En* is lower, and the *Ep* and μ_3 are higher for the melanoma. It means that they are characterized by less uniform images, with a higher disorder in terms of reflectance and a histogram more skewed than those of nevus. However, it can be appreciated that the mean reflectance of the melanoma is higher than that of the nevus, but this is not contradictory to the behavior of the average reflectance of both populations shown in Fig. 3, since the wavelength at which data is more entangled is just after 1200 nm.

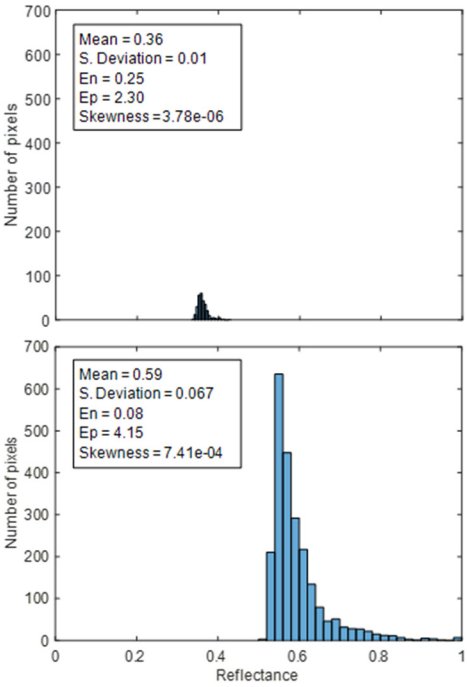

Figure 4. *Histograms of reflectance at 1214 nm of a nevus (top) and a melanoma (bottom) lesion.*

From the preliminary analysis of the reflectance and the parameters related to the histograms, it is clear that they can provide useful spectral and textural information of skin lesions and could be used as classifiers for predicting malignancy of a lesion.

As an example of this, Fig. 5 shows some plots of parameters which might allow for a classification of skin lesions. In particular, those that showed some tendencies that can be used for the classification of nevi and melanomas were:

- The spectral absorbance in terms of average at 1615 nm: *Mean of log(Refl$_{1615}$)*(Fig. 5 top).
- The spectral reflectance in terms of standard deviation at 1214 nm: *Standard Deviation of Refl$_{1214}$* (Fig. 5 bottom).

The plots show that for the two parameters some nevi tend to have values that stand out from the cloud of points in between the thresholds. Nevi are green points from 2 to 29 and melanomas are orange from 30 to 40.

With this initial classification algorithm based on these two parameters in which the lesions in between the thresholds are considered benign, none of the 11 melanomas were misclassified (100% sensitivity) but a 50% of nevi were misclassified as malignant though. Here, sensitivity or true positive rate is the proportion of melanomas correctly identified and the specificity or true negative rate is the probability of detecting nevi.

Among 180 descriptors, it was possible to find combinations that lead to optimizing the number of parameters that were able to classify the total number of melanomas and as much nevi as possible. This was done by creating a Matlab R2015a based code to which the manual thresholds for each parameter were introduced and it automatically retrieves the parameters that are able to classify all melanomas and at the same time misclassify the least number of nevi possible. The parameters that exhibited a more accurate classification of lesions were (Fig. 6):

- The spectral reflectance in terms of entropy at 1340 nm: *Ep Refl$_{1340}$ – Skin* (Fig. 6 top). For this parameter, the mean reflectance of a region of the skin without lesion was subtracted to the reflectance of the lesion before the calculation of the entropy.
- The spectral absorbance in terms of the minimum at 1340 nm: *Min log(Refl$_{1340}$)*(Fig. 6 center-top).
- The spectral reflectance in terms of mean at 1613 nm: *Mean Refl$_{1613}$* (Fig. 6 center-bottom).
- The spectral absorbance in terms of entropy at 995 nm: *Ep log(Refl$_{995}$)* (Fig. 6 bottom).

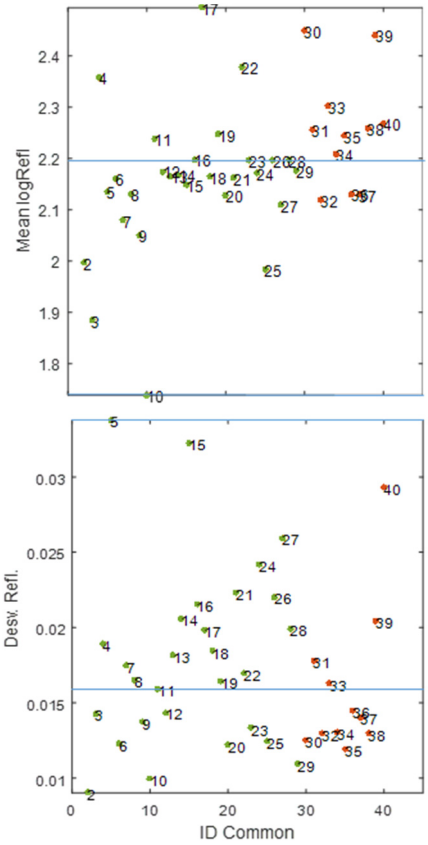

Figure 5. *Mean of log(Refl$_{1613}$) (top) and standard deviation of Refl$_{1214}$ (bottom). The green points correspond to nevi while those orange to melanomas. Both thresholds were defined experimentally to best discard melanomas from the cloud of nevi. ID refers to the identifier of each lesion.*

With these four parameters it was possible to classify the total number of melanomas (100% sensitivity) and only 7 nevi out of the 28 were misclassified (75% of specificity). The criterion used was the following one: once a lesion appeared to be out of the thresholds, it was considered a melanoma.

This criterion was taken because classifying malignant lesions out of the thresholds could lead us to misdiagnose nevus, but will not lead us to misdiagnose melanomas as benign lesions.

Present work is devoted to increase the number of both benign and malignant lesions included in the analysis to be able to set proper thresholds to perform the classification.

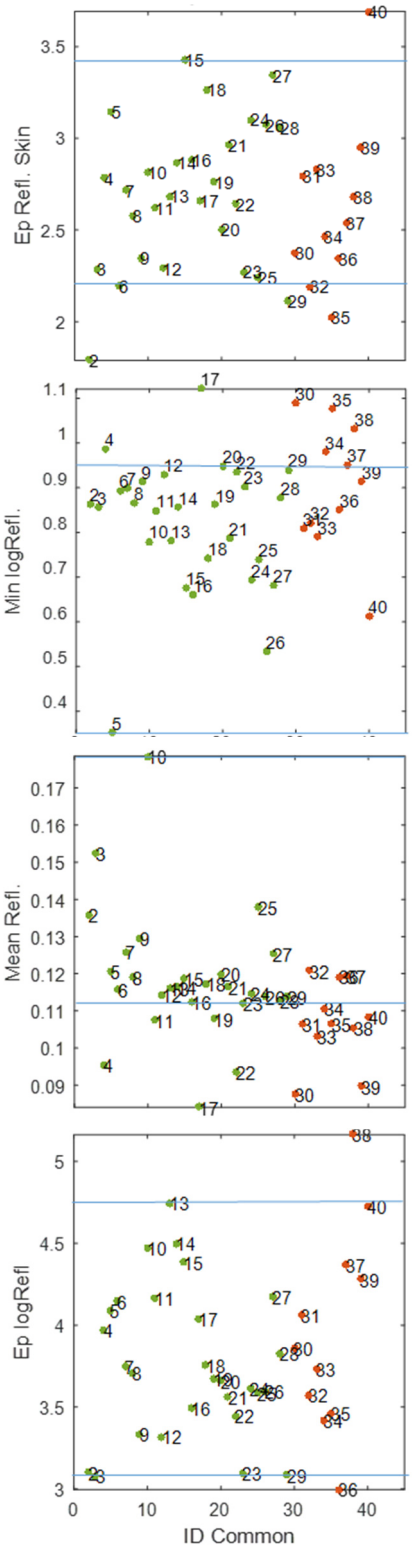

Figure 6. *Ep Refl$_{1340}$–Skin (top), Min log(Refl$_{1340}$)(center-top), Mean Refl$_{1613}$ (center-bottom) and Ep log(Refl$_{995}$)(Fig. 6 bottom). The green points correspond to nevi while the orange ones to melanomas. Both thresholds were defined experimentally to best discard melanomas from the cloud of nevi. ID refers to the identifier of each lesion.*

Conclusions

A handheld multispectral imaging system in the infrared range was developed for the detection of skin cancer. These preliminary results show the potentiality of the technique to discriminate between nevi and melanomas from the spectral and textural information available in the IR range. As already stated, present work focuses in increasing the number of lesions included in the analysis. The challenge expected is to obtain good classifiers among the descriptors with a significantly greater amount of lesions to properly establish the thresholds.

Future work will also be focused in analyzing other parameters beyond reflectance images such as the goodness-of-fit coefficient and empirical parameters based on spectral characteristics of chromophores and other components of the skin.

Acknowledgements

This research was supported by the Spanish Ministry of Economy, Industry and Competitiveness under the grant DPI2014-56850-R and the European Commission.

References

[1] P. Melia. (2017, Feb 20). *The Skin Cancer Foundation* [Online]. Available: http://www.skincancer.org.

[2] R. Stern, "Prevalence of a History of Skin Cancer in 2007," Arch. Dermatol., vol. 146, no. 3, pp. 279-282, 2010.

[3] Cancer Research UK. (2017, Feb 20). *Tests for skin cancer* [Online]. Available: http://www.cancerresearchuk.org/about-cancer/skin-cancer/getting-diagnosed/tests-diagnose.

[4] S. Tomatis, M. Carrara, A. Bono, C. Bartoli, M. Lualdi, G. Tragni, A. Colombo, and R. Marchesini, "Automated melanoma detection with a novel multispectral imaging system: results of a prospective study," Phys. Med. Biol., vol. 50, no. 8, pp. 1675-1687, 2005.

[5] I. Kuzmina, I. Diebele, D. Jakovels, J. Spigulis, L. Valeine, J. Kapostinsh, and A. Berzina, "Towards noncontact skin melanoma selection by multispectral imaging analysis," J. Biomed. Opt., vol. 16, no. 6, pp. 060502-060502, 2011.

[6] A. Bekina, I. Diebele, U. Rubins, J. Zaharans, A. Derjabo, and J. Spigulis. "Multispectral assessment of skin malformations using a modified video-microscope," Latvian Journal of Physics and Technical Sciences, vol. 49, no. 5, pp. 4-8, 2012.

[7] X. Delpueyo, M. Vilaseca, S. Royo, M. Ares, F. Sanabria, J. Herrera, F. Burgos, J. Pujol, S. Puig, G. Pellacani, J. Vázquez, G. Solomita, and T. Bosch, "Handheld hyperspectral imaging system for the detection of skin cancer," in Midterm Meeting of the International Colour Association, Tokyo, Japan, 2015.

[8] M. Ares, S. Royo, M. Vilaseca, J.A. Herrera, X. Delpueyo, F. Sanabria, "Handheld 3D Scanning System for In-Vivo Imaging of Skin Cancer" in 5th International Conference on 3D Body Scanning Technologies, Lugano, Switzerland, 2014.

[9] S.K. Özdemir, S. Shinohara, S. Tamkamiya, H. Yoshida, "Noninvasive blood flow measurement using speckle signals from a self-mixing laser diode: in vitro an in vivo experiments", Opt. Eng., vol. 39, no. 9, pp. 2574-2580, 2000.

[10] G. Pellacani, P. Guitera, C. Longo, M. Avramidis, S. Seidenari, S. Menzies, "The impact of In Vivo Reflectance Confocal Microscopy for the Diagnostic Accuracy of Melanoma and Equivocal Melanocytic Lesions", J. Invest. Dermatol. vol. 127, no. 12, pp. 2759-2765, 2007.

[11] G. Ritter, J. Wilson, Handbook of Computer Vision Algorithms in Image Algebra, 2nd ed., Boca Raton: CRC Press, 2000.

[12] X. Delpueyo, M. Vilaseca, S. Royo, M. Ares, F. L. Rey-Barroso, Sanabria, S. Puig, G. Pellacani, F. Noguero, G. Solomita, and T. Bosch, "Multispectral imaging system based on light emitting diodes for the detection of melanomas and basal cell carcinomas: a pilot study," J. Biomedical Optics, 2017.

Author Biography

Laura Rey received her BSc Degree in Biomedical Engineering from the University Carlos III of Madrid, where she made some research about the new applications of spectroscopy. She received her MSc in Photonics from the Technical University of Catalonia (UPC) in 2016. She is currently working as a researcher at the CD6-UPC. Her work has focused on skin cancer diagnosis by multiespectral techniques.

Francisco J. Burgos-Fernández received his Degree in Optics and Optometry in 2008, his MSc in Photonics in 2011, and his Ph.D. in Optical Engineering in 2016 from the UPC. He is currently working as a postdoctoral researcher at the CD6-UPC. He has participated in several research projects related to spectral imaging for cultural heritage, automotive industry and skin cancer diagnosis, industrial colorimetry, and radiometry.

Xana Delpueyo received her Degree in Optics and Optometry in 2011 and her MSc in Vision Science in 2013 from the UPC. She is currently a student of the Ph.D. in Optical Engineering of the UPC. Her work has focused on spectral imaging for skin cancer diagnosis and paleontology.

Miguel Ares received his Ph.D. in Optical Engineering in 2009 from the UPC. He is currently a postdoctoral research fellow in CD6-UPC working in the development of technologies and methods based on optical and computer vision techniques for 3D scanning. He has participated in public (8) and private (7) funded research projects and have published 4 articles 'peer-reviewed' as a first author and 2 patents.

Santiago Royo received his Ph.D. in Applied Optics in 1999 from the UPC. He is currently Associate Professor at UPC and Director of the CD6. He has participated and led research projects in optical metrology and engineering, leading him to publish over 50 full-text publications and 10 patents, five of them licensed. He is co-founder of three photonics-based spin-off companies: SnellOptics, ObsTech SpA, and Beamagine S.L.

Josep Malvehy received his Ph.D. in Genetics and Dermoscopy of melanoma in 2006 from the University of Barcelona (UB). He is currently consultant dermatologist of the Hospital Clinic of Barcelona and Associated Professor at the UB since 2010. His work has focused on non-invasive methods for the diagnostics of skin cancer and other skin diseases including biophotonic methods since 1998.

Susana Puig received her Ph.D. in Genetics of melanoma in 2000. She is the Chief of the Department of Dermatology at the Hospital Clinic of Barcelona and Associated Professor of the UB since 2010. Her work has focused on diagnostic methods of skin cancer with special interest in Dermoscopy, confocal Microscopy and other photonic techniques since 1996.

Meritxell Vilaseca received her BSc Degree in Physics in 2000 from the Autonomous University of Barcelona and her Ph.D. in Physics in 2005 from the UPC. She completed her Degree in Optics and Optometry in 1996 at the UPC. She is currently working as Associate Professor at the UPC and as a researcher at the CD6-UPC. She has participated and led several research projects related to spectral imaging, industrial colorimetry, and visual optics.